Martinez, J. O., Genoves Guzman, B., & Garcia Armada, A. (2026). Correlation and drop velocity in fluid antenna systems: Modeling and performance. IEEE Journal on Selected Areas in Communications, 44, 1322–1334.

DOI: https://doi.org/10.1109/jsac.2025.3617473

Correlation and Drop Velocity in Fluid Antenna Systems: Modeling and performance

Javier Otero Martinez, *Student Member, IEEE*, Borja Genoves Guzman, *Senior Member, IEEE* and Ana Garcia Armada, *Fellow, IEEE*

***Abstract*—Emerging technologies like Fluid Antenna Systems (FAS) are important ingredients toward new generation communications. In particular, we focus on systems based on the reconfigurability capabilities of liquid antennas, which are a subset of FAS that use a liquid as their main conductor. Despite recent pertinent advances in the field, the reconfiguration speed was not directly addressed in the literature, as it is assumed to be very high in most works. However, it is a crucial parameter that defines the system's capabilities and performance bounds. In addition, a few approaches to spatial correlation modeling are presented here that are also needed for a holistic performance evaluation. Hence, a numerical methodology is proposed to realistically model both parameters. Performance metrics are also addressed, which aid in identifying and comprehending the system's strengths and weaknesses. The importance of these models and metrics is showcased by reconfiguring the FAS, proposing several algorithms and illustrating their features. As a result, we show that it is possible to obtain a realistic performance evaluation for FAS and improve currently available models and performance to further progress on this topic.**

***Index Terms*—Fluid Antenna, Reconfigurable Antenna, Spatial Correlation**

I. Introduction

New generation communication systems are intended to change our way of interacting with information and society. 6G technologies pursue the possibility of a new communications paradigm with improved dependability and connectivity. Without question, in order for our current systems to deliver the services that are envisaged, they must be enhanced and supplemented with new designs and methods. One of these emerging technologies are Fluid Antenna Systems (FAS) [1], also known as Movable Antennas (MAs) [2]. Regardless of the name used to refer to them, these devices are meant to take advantage of the spatial dimension to possibly achieve extra degrees of freedom, which can be potentially exploited to significantly improve the performance of a whole communication system. Accordingly, FAS must be able to reconfigure themselves in real time to match a set of different requirements defined by the considered application.

One particular subset of FAS are systems based on liquid antennas. They aim to achieve reconfigurability by using a metallic conducting material that is liquid at room temperature. In our case, we focus on the eutectic alloy of indium and gallium (eGaIn), which presents a conductivity that is an order of magnitude better than its traditional competitor, mercury, in spite of being non-toxic, non-inflammable and non-radioactive [3]. In consequence, there is an increasing motivation to research, understand and potentially increase the use cases of eGaIn-based liquid antennas [4], [5]. In any case, the models and performance measures that we are presenting here are applicable for the more general class of FAS, so we will refer to them in the following.

Several publications can be found that illustrate the advantages of Fluid Antennas (FA) when compared to traditional systems [4], introducing different ways of optimizing their use for widely spread technologies such as Multiple Input Multiple Output (MIMO) [6] or beamforming [7]. It has also been studied how to combine them with other alternative emerging technologies, such as Reconfigurable Intelligent Surfaces (RIS) [8], Non-Orthogonal Multiple Access (NOMA) [9] or Integrated Sensing And Communication (ISAC) [10]. A comprehensive tutorial can be found in [11], where these and other references are explored and summarized.

Not only ways to understand and improve communications theoretical concepts with FAS are being explored. There have also been some works focused on physical implementations as well, such as [12] or [13]. However, studies about hardware implementations and analytical designs are rather disconnected, a weakness that we address here by focusing on a realistic approach to the system modeling that takes into account the results from recent experiments. In that regard, some of our preliminary tests, exemplified in Fig. 1, point out that reconfiguration speeds in the range of 10 - 100 mm/s can be achieved using continuous electrowetting (CEW) [14]. Applying this technique to FAS would allow us to move a volume of liquid metal without mechanical pumps, but using electric impulses only. This would be convenient to easily displace the antenna element (in many cases just a drop of metal) to any position, raising the number of feasible applications by eliminating the need for any mechanical devices.

As stated above, many authors are exploring the performance of FA as well as their use cases. In our view, further progress cannot be made if the models are too idealistic. We need the ability to account for reconfiguration speeds and their relation with transmission scenarios. Therefore, the main contributions of this article are the following:

- We describe a realistic system model that is able to capture several typically found correlation scenarios and their impact on the performance of the communication

All authors are with Signal Theory and Communications Department of Universidad Carlos III de Madrid. This work has been partially funded by projects HE 101192080 (6G-LEADER) and PID2023-147305OB-C31 (SOFIA-AIR) by MCIN/ AEI/10.13039/501100011033/ERDF, UE, funded by the European Union, and by project PID2024-156038OA-I00 (HOLIFI6G) by MICIU /AEI /10.13039/501100011033 / FEDER, UE. Views and opinions expressed are however those of the author(s) only and do not necessarily reflect those of the European Union. Neither the European Union nor the granting authority can be held responsible for them. Borja Genoves Guzman has received funding from Ramón y Cajal grant RYC2023-042518-I, funded by MCIU/AEI/10.13039/501100011033 and FSE+.

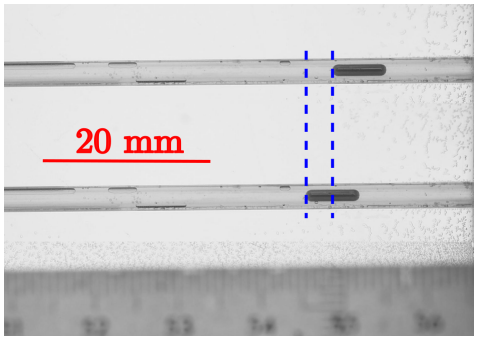

Fig. 1. Example of eGaIn displacement using electrowetting. Two frames of a video of a typical experiment and a ruler added as a reference. An electric voltage is applied throughout the tube, moving the drop using only 1 V.

system. We also discuss the relevance of the drop velocity, as it is an important parameter that has not been considered before. Both correlation and drop velocity are key parameters to grasp the real capabilities of FA; therefore, they should be accurately captured by the model. Considering realistic scenarios and velocities would boost the feasibility of actual FA studies towards their successful implementation.

- We explain accurate and practical models to account for the port correlation, including a numerical method based on Auto-Regressive Moving-Average (ARMA) filtering. This is a refined version of our preliminary work [15].
- We present different algorithms for FA reconfiguration. Since they require different levels of channel state information (CSI), they allow navigating from more idealistic scenarios to more realistic ones. Henceforth, several parameters of the system can be adapted and their influence is highlighted.
- We propose the use of alternative metrics in addition to the outage probability (OP). We show that only considering the OP may not be enough to fully characterize some emerging use cases of FA, such as the case of liquid antennas.

In summary, we contribute to state-of-the-art modeling of FAS, which is critical for the evolution of the topic and to understand the performance of suitable use cases for these technologies.

The reminder of this paper is structured as follows. After this introduction, Section II describes the system model of the proposed FA. In particular, we focus on the FA model in agreement with a possible physical implementation in Section II-A and provide a generic description of spatial correlation in Section II-B. Section III addresses the state-of-the-art analytical correlation modeling for FA and presents three different methods in depth. Several approaches to port selection are detailed in Section IV. Section V defines the performance metrics that will be used for comparison. Section VI presents the numerical results, showing the accuracy of the methodologies and the performance analysis with the proposed metrics. Finally, Section VII presents the conclusions and future work.

Notation: The expected value is denoted as $\mathbb{E}[\cdot]$. For random processes X, Y we define the mean, μ, as $\mathbb{E}[X]$ and the variance, σ_X^2, as $\mathbb{E}\left[(X-\mu)^2\right]$. Note that the variance can be seen as the covariance of one variable with itself. Therefore, the Greek letter σ is commonly used for both as $\sigma_{XY} = \mathbb{E}[XY] - \mathbb{E}[X]\,\mathbb{E}[Y]$. Correlation can be seen as a normalization of the covariance but their numerical value is the same if both processes have zero mean and unit variance, since $\rho_{XY} = \sigma_{XY}/\sigma_X\sigma_Y$. Vectors, matrices and scalar quantities are defined using boldface lowercase, boldface uppercase and regular lowercase letters. $\mathcal{CN}(0, \sigma_\alpha^2\mathbf{\Sigma})$ represents the circularly symmetric, zero-mean complex normal distribution with covariance matrix Σ. $J_0(\cdot)$ is the zero-order Bessel function of the first kind. $\mathbf{I}_z$ is the $z \times z$ identity matrix. j denotes the imaginary unit.

II. System Model

In this section we describe the topology of the proposed FA and the spatial correlation modeling.

A. FA Model

We propose a FA model that is similar to the one proposed in [1] and consistent with some hardware implementations of liquid antennas [16]. We consider a device that would act as a single antenna element for reception, employing a single radio-frequency (RF) chain. This device consists of a tube that serves as a container for a drop of eGaIn. This drop, which acts as an antenna, is able to move inside the tube with speed v_c, to reach a set of N defined configurations which are often referred to as *ports*. The position of the drop can be computed simply as

$$n(t) = n_0 \pm v_c t, \tag{1}$$

where $n(t)$ is an arbitrary position, n_0 is the initial position, v_c is the reconfiguration speed —which is directly mapped to drop speed— and t is the temporal variable that is omitted from now on for conciseness.

The tube has a fixed length of L. An illustrative scheme of the FA model can be seen in Fig. 2. As a consequence, the proposed eGaIn antenna would be able to capture incoming signals that have experienced different propagation channels depending on the position of the drop. This represents an additional degree of freedom toward highly reconfigurable antenna devices. In our model, ports are continuous, meaning that the space between them is negligible. We assume that obtaining CSI of a particular port is a much faster process than the drop speed. The position of the drop is always known and it is assumed to accelerate instantaneously.

In principle, the higher the number of ports, the greater the diversity is, but undoubtedly, since ports can be very close, a high spatial correlation is expected among them. In accordance, such a correlation may limit the potential of this configuration for communications. Accounting for spatial correlation using pure analytical tools would be highly desirable [4]. However, keeping mathematical tractability may compromise the resulting performance indicators. Some solutions rely on approximated correlation coefficients that either have a difficult physical interpretation or are exclusive to the

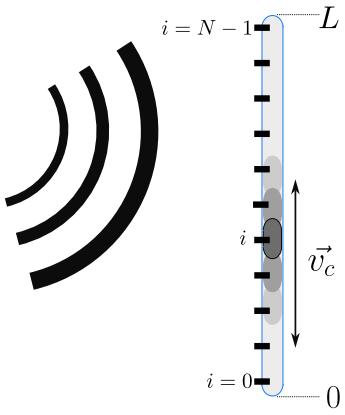

Fig. 2. Model scheme of the proposed antenna.

particular correlation scenario under study, and consequently not general enough. In this work we model spatial correlation using three different methods:

- An analytical approximation following [17], which would serve as a reference to our numerical models. It is based on a Singular Value Decomposition (SVD) of the covariance matrix that allows selecting the dominant eigenvalues to produce the desired correlation function. It will be summarized in Section III-A.
- A numerical solution based on taking samples from a multivariate Gaussian distribution, detailed in Section III-B. This technique will be referred to as Sampling a Multivariate Distribution (SMD) below. It is equivalent to the previous method without decomposing the covariance matrix, and can be applied to obtain numerical solutions.
- An alternative numerical solution based on ARMA filtering. It will be described in Section III-C.

First, let us define the spatial correlation of interest, and review how it is usually modeled in the literature.

B. Spatial correlation in FA

As one might expect, the correlation experienced by a signal due to the propagation channel in FA is similar to that of a classical multi-antenna system. However, in the case of FA, N can be arbitrarily large, and hence the possible antenna ports are very close to each other. Spatial correlation is often addressed in the literature with a particular focus on multi-antenna or MIMO systems. In consequence, it is commonly assumed that two antennas are uncorrelated for spacings larger than $\lambda/2$. However, this is not the case of interest for FA, as many ports can be placed within this distance. Appropriately modeling the spatial correlation within distances smaller than $\lambda/2$ is key to not over- or under-estimating the capabilities of FAS. We describe in the following the correlation between ports and the classical approach to model it.

A spherical reference system is used (see Fig. 3). Therefore, any point in the space is described as $\mathbf{r} = (r, \varphi, \theta)$. With r being the distance to the reference point, $\varphi \in [0, 2\pi)$ the azimuth angle and $\theta \in [0, \pi)$ the elevation angle. For simplicity, a 2D space is considered which corresponds to a

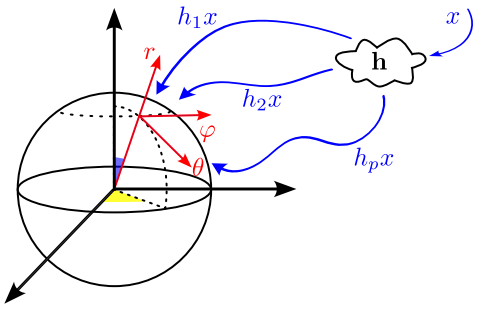

Fig. 3. Coordinate system with incoming signals. $h_p x$ represent the contribution of the p-th path to the received signal.

fixed value of $\theta = \pi/2$ [18]. If a narrowband signal x is transmitted through a flat fading channel, the received signal y at the i-th port has the form

$$y_i = h_i x + w. \tag{2}$$

Here, w denotes the complex additive Gaussian noise (AWGN) with zero mean and variance of σ_w^2, and h_i the channel coefficient associated to the i-th port which in general follows a circularly symmetric complex Gaussian distribution, also with zero mean and variance σ_h^2. The instantaneous signal to noise ratio (SNR) of a given port i, Γ_i, is computed as

$$\Gamma_i = \mathbb{E}\left[|x|^2\right] \frac{|h_i|^2}{\sigma_w^2}, \tag{3}$$

where the expectation is taken over time.

The value of the channel coefficient at an arbitrary position $\mathbf{r}_i$ is given by the superposition of plane waves (paths) as

$$h_i = \int \alpha\, G(\varphi) e^{j\,\mathbf{r}_i\,\mathbf{k}(\varphi)}\, d\varphi, \tag{4}$$

where α is the associated complex path gain, $G(\varphi)$ is the antenna radiation pattern, $\mathbf{k} = 2\pi/\lambda\,(\cos\varphi, \sin\varphi)$. If a finite number of paths P is assumed, the integral becomes a summation as

$$h_i = \sum_{p=1}^{P} \alpha_p\, G(\varphi_p) e^{j\,\mathbf{r}_i\,\mathbf{k}(\varphi_p)}, \tag{5}$$

where the subindex p denotes the p-th path of the incoming signal that is scattered when affected by the environment. The total received power is distributed between the paths according to their gain, which follows an independent random variable with zero mean and variance σ_α^2/P.

Rayleigh fading results when assuming that the angles of arrival (AoA) of the different paths are independent and identically distributed. Accordingly, if two antenna elements $\mathbf{r}_n$, $\mathbf{r}_m$ are close enough for the path gains and AoA to be the same (i.e. spatial correlation exists), then

$$\begin{aligned} \rho_{n,m}^2 &= \mathbb{E}[h_n h_m^*] \\ &= \sigma_\alpha^2\, \mathbb{E}\left[|G(\varphi)|^2 e^{j(\mathbf{r}_n - \mathbf{r}_m)\mathbf{k}(\varphi)}\right]. \end{aligned} \tag{6}$$

Isotropic antennas are commonly assumed, therefore $|G(\varphi)|^2 = 1$. Hence the spatial correlation for this model depends only on the different AoA which are imposed by the environment. If the scatterers are placed on a ring close to the

receiver, the incoming signal's AoA are uniformly distributed, which is the assumption leading to the commonly known as Jakes' model [19]. Introducing these conditions into (6) yields

$$\rho_{n,m}^2 = \sigma_\alpha^2 \, J_0(\, 2\pi \parallel \mathbf{r}_n - \mathbf{r}_m \parallel / \lambda \,), \tag{7}$$

with $J_0(\cdot)$ being the zero order Bessel function of the first kind. This Jakes' model is equivalent to the 2D Clarke's model [20]. This result implies that the signals at two antennas separated by $\lambda/2$ are considered to be uncorrelated. Here, our goal is to accurately capture the characteristics of the propagation channel that have an impact on the FA behavior, with a particular focus on very short antenna port spacings.

Equation (7) is an example of *correlation function*, as it contains all the possible correlation values as a function of the distance between ports. Therefore, since the geometry of the FA is fixed, this correlation function depends only on the environment: scatterers distribution, AoA, radiation pattern of the elements, etc. Undoubtedly, Jakes' model emerges as the most known correlation model within the community. However, the assumptions made might not always be convenient or realistic.

The 3$^{\text{rd}}$ Generation Partnership Project (3GPP) proposes different correlation models [21] that represent scenarios of interest and can be translated into correlation functions using analytical or numerical methods present in the literature. Their computation is not directly addressed in this work, but some scenarios are compared using the expressions found in [22], which are included below. For simplicity, a 2D scattering environment is considered. Then the spatial correlation is

$$\rho(r_n - r_m) = \sum_{k=-\infty}^{\infty} j^k \, \chi_k \, J_k \left(\frac{2\pi}{\lambda} \, ||r_n - r_m|| \right) e^{jk\varphi_{nm}}, \tag{8}$$

where φ_{nm} is the angle of the vector connecting r_n and r_m and χ_k is generally defined as

$$\chi_k = \int_0^{2\pi} \mathcal{P}_{(\varphi)} \, e^{jk\varphi} \, d\varphi, \tag{9}$$

with $\mathcal{P}_{(\varphi)}$ being the power distribution function. Furthermore, [22] proposes concise values for χ_k depending on the correlation environment. It proves that, for uniformly distributed values over an angle of 2π, the result converges to $\rho(r_n - r_m) = J_0(k \, ||r_n - r_m||)$ that corresponds to the Jakes' Model. Moreover, if energy is arriving from a fraction of the azimuthal range only, $(\varphi_0 \pm \Delta)$, the calculation changes to

$$\chi_k = e^{-jk\varphi_0} \, \mathrm{sinc}(k\Delta). \tag{10}$$

According to the 3GPP, a Laplacian distribution may be adequate for channel modeling [21], with a power distribution given by

$$\mathcal{P}_{(\varphi)} = \frac{Q}{\sigma\sqrt{2}} \exp \left[\frac{-|\varphi - \varphi_0|\sqrt{2}}{\sigma} \right]. \tag{11}$$

Here, Q is a normalization parameter, σ is the Laplacian scale parameter and $|\varphi - \varphi_0| \leq \pi/2$ describes the azimuthal range. In consequence, the resulting expression is

$$\chi_k = e^{jk\varphi_0} \, \frac{1 - F_k \beta (-1)^{\lceil k/2 \rceil}}{(1-\beta)(1 + \sigma^2 k^2/2)} \tag{12}$$

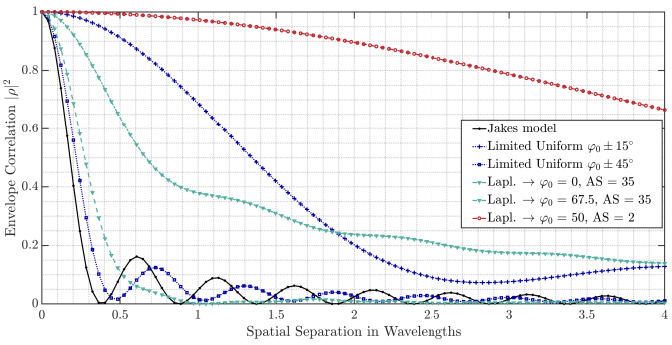

Fig. 4. Different correlation functions corresponding to Jakes' model, Laplacian distribution and uniformly distributed scatterers over the azimuth angle $\Delta = 30°$.

with

$$\begin{aligned} \beta &= e^{-\pi/\sqrt{2}\sigma}, \\ F_k &= 1 \quad \text{for } k \text{ even}, \\ F_k &= \frac{k\sigma}{\sqrt{2}} \quad \text{for } k \text{ odd}. \end{aligned} \tag{13}$$

In the case of this distribution, the angular spread (AS) is given by

$$\mathrm{AS} = \sqrt{\frac{1}{1-\beta} \left(\sigma^2 - \frac{\beta}{4} (\pi^2 + 4\sigma^2 + \sqrt{8}\pi\sigma) \right)}. \tag{14}$$

Figure 4 shows some of the correlation functions presented above. For simplicity, 2D functions are considered in this article, but the expressions for 3D environments are also available in the literature.

For this application, a covariance matrix, $\mathbf{\Sigma} \in \mathbb{C}$ is defined such that it contains the covariances among all the ports. $\mathbf{\Sigma}$ is commonly assumed to have a Toeplitz structure (each diagonal descending element is constant). If that is the case, $\mathbf{\Sigma}$ is built by sampling values from the correlation function [23] as

$$\mathbf{\Sigma}^{R \times R} = \begin{bmatrix} \rho(0) & \rho(1) & \dots & \rho(R-1) \\ \rho(1) & \rho(0) & \dots & \rho(R-2) \\ \vdots & \vdots & \ddots & \vdots \\ \rho(R-1) & \rho(R-2) & \dots & \rho(0) \end{bmatrix} \tag{15}$$

where R is the length of the correlation function ρ. The only constraint for $\mathbf{\Sigma}$ to be a valid covariance matrix in terms of mathematical tractability is to be semi-definite positive, regardless of the features of the environment (2D, 3D, number of scatterers, etc).

III. Modeling Correlated FAS

The preceding section introduced various expressions to characterize the correlation functions, while this section describes how to use these expressions to model the environment. Three different methodologies are presented, amenable to analytical or numerical solutions.

Firstly, analytical approaches rely on comprehensive mathematical expressions that produce one desired metric or parameter. Several different expressions need to be derived for every parameter of interest which, altogether, define the

environment. For the particular case of spatial correlation in FA, much effort has been put to obtain such expressions [4], but closed form, simple equations are not always available.

Secondly, numerical methods aim to address the whole scenario to evaluate the different parameters of interest. In general, they are more comprehensive and allow computing different outcomes at once, at the cost of higher computational power and loss of conciseness. We present two different numerical methods.

A. Analytical Block Correlation Model

Inspired by the parallelism between time and space, the authors of [17] characterize the spatial correlation using a block diagonal matrix for the covariance matrix $\mathbf{\Sigma}$, providing a good tradeoff between mathematical tractability and accuracy for most common use cases. This $\mathbf{\Sigma}$ consists of a set of different blocks with different size according to the importance of their associated eigenvalues. Although the correlation value within each block is constant, it differs from one block to another. They demonstrate in [17] that $\mathbf{\Sigma}$ is dominated by a few of its original eigenvalues. Therefore the estimation of $\mathbf{\Sigma}$, denoted as $\widetilde{\mathbf{\Sigma}}$, consists of B different blocks $\mathbf{A_b}$ as

$$\widetilde{\mathbf{\Sigma}} = \begin{bmatrix} \mathbf{A_1} & 0 & \dots & 0 \\ 0 & \mathbf{A_2} & \dots & 0 \\ \vdots & \vdots & \ddots & \vdots \\ 0 & 0 & \dots & \mathbf{A_B} \end{bmatrix}, \tag{16}$$

with each sub-block $\mathbf{A_b}$ having the form

$$\mathbf{A_b} = \begin{bmatrix} 1 & \mu^2 & \dots & \mu^2 \\ \mu^2 & 1 & \dots & \vdots \\ \vdots & \vdots & \ddots & \mu^2 \\ \mu^2 & \dots & \mu^2 & 1 \end{bmatrix} \text{ with } b = 1, 2 \dots B. \tag{17}$$

By choosing the parameter μ close to 1, each block produces a single dominant eigenvalue, so the block works as an approximation to the corresponding eigenvalue of $\mathbf{\Sigma}$. Evidently, some of the least dominant eigenvalues are discarded in this process to make an approximation. For that reason, the paper defines a threshold (ς_{th}) to decide which eigenvalues are dominant and which are to be discarded. In summary, this method aims to produce a good estimation of $\mathbf{\Sigma}$, $\widetilde{\mathbf{\Sigma}}$, such that

$$\underset{B,\, L_B,\, \mu}{\arg\min}\, \text{dist}\left(\mathbf{\Sigma}, \widetilde{\mathbf{\Sigma}}\right), \tag{18}$$

where $\text{dist}(\cdot)$ is a distance metric between the approximated and true covariance matrices. According to [17], the choice of this metric is highly non-trivial. Moreover, it is hard to predict its impact on the final approximation. For numerical evaluation, channel instances are generated following this model as $\mathbf{h} \sim \mathcal{CN}(0, \sigma_\alpha^2 \widetilde{\mathbf{\Sigma}})$.

This methodology greatly reduces the structure of $\mathbf{\Sigma}$ which, as the authors prove, is really convenient for its later use in analytical expressions. Once obtained, the computation of the OP, for instance, is straightforward as shown in [17]. Nevertheless, if some other metrics are to be computed, their tailored expressions would have to be derived, and the parameters would need to be adjusted for the algorithm to converge to an accurate solution. Moreover, for some scenarios, the resulting correlation needs to be compared with a known distribution to iteratively mitigate the approximation errors. This is done for Jakes' model in [17], but it may not be straightforward in other cases. In summary, this methodology facilitates the analytical performance, but adjusting the parameters for different channel models may be challenging. This motivates the following alternate numerical methods.

B. Numerical Method I: Sampling a Multivariate Distribution

In this method, denoted as SMD, the propagation channel coefficients are generated by taking samples of a normal distribution as $\mathbf{h} \sim \mathcal{CN}(0, \sigma_\alpha^2 \mathbf{\Sigma})$. The covariance $\mathbf{\Sigma}$ is the identity matrix for uncorrelated environments. Otherwise, the elements of $\mathbf{\Sigma}$ need to account for the correlation. If the correlation function is known, the covariance matrix $\mathbf{\Sigma}$ can be easily computed according to (15).

To generate correlated samples of a normal distribution, we resort to the Cholesky decomposition that allows expressing the covariance matrix as [24]

$$\mathbf{\Sigma} = \mathbf{C}\mathbf{C}^T, \tag{19}$$

where $\mathbf{C}$ is the outcome of the decomposition. By definition, if $\mathbf{X}$ corresponds to uncorrelated values $\mathbf{X} \sim \mathcal{CN}(0, \mathbf{I_N})$, then

$$\mathbf{h} = \mathbf{C}\mathbf{X} \tag{20}$$

contains the correlated values according to $\mathbf{\Sigma}$. This numerical method can be used to compute a large set of correlated channel coefficients representing the desired environment, to be used in numerical evaluations through the Montecarlo method [23]. Note that, by definition, the covariance matrix will be semidefinite positive and symmetrical, which guarantees a single form for $\mathbf{C}$.

C. Numerical Method II: ARMA Filtering

The third method to model the spatial correlation in FA consists in generating a complex white Gaussian distributed vector which is processed afterwards to match a desired correlation function. This can be done using ARMA filtering techniques according to [23]. Therefore, no $\mathbf{\Sigma}$ will be computed in this method. The only input parameter is the correlation function. The definition of an ARMA process X_t of order (s, q) is

$$X_t = -\sum_{k=1}^{s} a_k X_{t-k} + \sum_{k=1}^{q} b_k W_{t-k}, \tag{21}$$

where W_t is a white noise process with unit variance and zero mean. It is proven that for an ARMA process, its associated correlation coefficients ρ_x obey [25]

$$\rho_{q+l} + a_1 \rho_{q+l-1} + \ \dots \ + a_p \rho_{q+l-s} = 0, \tag{22}$$

where ρ_i is defined as

$$\rho_i = \mathbb{E}\left[X_t X_{t-k}\right] \tag{23}$$

with $l \geq 1$. Consequently, a set of linear equations with $1 \leq l \leq s$ can be solved to find the AR coefficients, a_k.

They are known as the modified Yule-Walker equations. There are different methods for the calculation of the MA process coefficients (of order q). In the frequency domain,

$$\frac{n(z)}{a(z)} \triangleq \sum_{k=1}^{\infty} \rho_k z^{-k}, \tag{24}$$

with $n(z) = n_1 z^{-1} + ... + n_p z^{-s}$. The MA spectrum is

$$S(z) = \frac{b(z)\, b(z^{-1})}{a(z)\, a(z^{-1})}, \tag{25}$$

$$S(z) \triangleq \sum_{k=-\infty}^{\infty} r_k\, z^{-k}$$

and its associated coefficients have the form [25]

$$\begin{aligned} &b(z)\, b(z^{-1}) = \\ &\quad n(z)\, a(z^{-1}) + r_0\, a(z)\, a(z^{-1}) + a(z)\, n(z^{-1}). \end{aligned} \tag{26}$$

As shown, MA coefficients are harder to compute. Therefore, for this application we focus on improving the AR stage at the cost of a suboptimal output [25]. There is plenty of literature on this topic and ARMA filtering design is out of the scope of this work. Nonetheless, the former reference explains that selecting the order of the process is key to achieving accurate results. The error is measured as [26]

$$\varepsilon(s) = \rho_{xx}(0) + \sum_{k=1}^{s} \rho_{xx}(-k), \tag{27}$$

where $\varepsilon(s)$ is the prediction error, $\rho_{xx}(k)$ the target correlation function and s the order of the ARMA process. Thus, it is needed to find the order at which ε is minimum. That is

$$\hat{s} = \arg\min_{s}\, \varepsilon(s) \tag{28}$$

having in mind that s has to be greater than N. Moreover, once the correct order of the process is reached, it is guaranteed that no higher values of s yield better performance [26]. We will minimize the order of the ARMA process according to this procedure.

Following these steps allows us to design a filter in such a way that after filtering a white random variable, it presents a given autocorrelation function. In other words, this transformation *correlates* a set of channel coefficients that would be otherwise uncorrelated —e.g. with a sufficiently large port spacing—.

D. Summary of correlation modeling

Every presented method facilitates the generation of correlated column vectors $\mathbf{h}$ of length equal to N, to represent a given correlation environment. These vectors are stacked horizontally to conform a channel matrix $\mathbf{H}$ of dimensions $N \times t_s$, with t_s being the number of time instants, as

$$\mathbf{H}_{(N\times t_s)} = \begin{bmatrix} h_{1,t_s=1} & h_{1,t_s=2} & \cdots \\ h_{2,t_s=1} & h_{2,t_s=2} & \cdots \\ \vdots & \vdots & \vdots \end{bmatrix}. \tag{29}$$

TABLE I
SUMMARY OF PROPOSED METHODS

	BLOCK	**ARMA**	**SMD**
Numerical	✗	✓	✓
Analytical	✓	✗	✗
ρ-dependent	✓	✓	✓
$\mathbf{\Sigma}$-dependent	✓	✗	✓
Matrix inverse or transpose	✓	✗	✓
Convolution	✗	✓	✗
Tunable parameters	✓	✓	✗
Method flexibility	✓	✓	✗
Simplicity	✗	✗	✓

This channel matrix represents the propagation environment, and it is the starting point for any numerical approach.

Whereas Block and SMD methods require the computation of the covariance matrix, ARMA does not. In turn, it requires the filter design and applying its associated convolution. In principle, both ARMA and Block methods require adjusting several parameters. This can imply increased complexity but offers the flexibility to closely adjust the desired output. On the other hand, SMD is quite straightforward when compared to the other two if correlation functions are easily mapped into covariance matrices. Table I summarizes the features of the proposed approaches.

IV. Port selection and FA Reconfiguration

The FA can be reconfigured by displacing the eGaIn drop to different ports, choosing the best one according to some optimization criterion. Different procedures are proposed in this section to illustrate the feasibility of port selection processes and the importance of considering the drop speed in their modeling. These algorithms are executed at every coherence time, and the starting point at one execution is the ending port at the previous one. Our goal is to show examples of the impact of moving the drop to reconfigure the CSI in a way that the communications specifications are satisfied.

Many sources such as [27] highlight the problem of retrieving trustworthy CSI in real time to be able to reconfigure the FA accordingly. A full sweep along the FA dimension takes a considerable amount of time, and the liquid metal will typically move much slower when compared to communication data rates. This would cause a critical loss of performance efficiency if the drop needs to travel along the whole device every time a CSI update is needed. And this is additional to other non-FA-specific problems, such as overhead due to obtaining CSI and computational load. Consequently, we propose three methods that vary in the degree of CSI knowledge and computational complexity.

It is assumed that, although each port offers a different CSI, those values are constant within a given coherence time T_c, which leads to different SNR values obtained if the drop is in contact with every port i (Γ_i of (3)). In such a coherence time, the drop can travel throughout the antenna device at a speed v_c. Let us define $\mathbf{t}$ as the vector containing all t_i, $\forall i$ values, where t_i is the time during which the drop is in contact with port i. Since ports are presumed to be continuous (i.e., there is

no vacant space between them), transmission is possible along all the route. For every method, an initial channel sweep is carried out, examining every port hence the algorithms start in the port with best SNR.

A. MAXSNR *algorithm*

We first assume an ideal scenario where the SNR values for all ports are known at all times, acting as an upper bound for the FA performance. The focus is on maximizing the average SNR over the coherence time defined as

$$\bar{\Gamma} = \sum_i \frac{t_i}{T_\mathrm{c}} \Gamma_i, \tag{30}$$

which will be our objective function. Note that the unknown variables are $t_i \, \forall i$, so the objective function is linear. An optimization problem can be solved with off-the-shelf software if constraints are linear, bilinear or quadratic, in both convex and non-convex optimization problems [28]. In the following, the constraints are analyzed, in order to propose a solution.

1) Bounding times at each port: The time a drop spends at each port is zero or greater than a minimum time t_min, defined as the time it takes for a drop to cross a port. If $L_\mathrm{port} = L/N$ is the port length, then $t_\mathrm{min} = L_\mathrm{port}/v_c$. This is a *disjunctive* constraint in optimization, meaning the variable can satisfy one of several conditions. This cannot be modeled directly with standard linear programming because the feasible region would be disconnected. Therefore, a new variable is created, $\mathbf{b}$, which is an array of binary variables b_i, indicating the ports that are selected by the drop within such coherence time, in such a way that $b_i = 1$ if port i is in contact with the drop during time t_i different to zero, or $b_i = 0$, otherwise. Thus the formulation is

$$b_i = \begin{cases} 0, & \text{if } t_i = 0 \\ 1, & \text{if } t_i > t_\mathrm{min} \end{cases}, \tag{31}$$

which can be linearized by following the big-M approach to turn this conditional statement into two linear inequalities [29], where M_1 is considered as an upper bound of t_i, i.e., $M_1 = T_\mathrm{c}$,

$$t_i \geq \frac{L_\mathrm{port}}{v_c} b_i, \forall i \tag{32}$$

$$t_i \leq M_1 \, b_i, \forall i. \tag{33}$$

Note that, when $b_i = 1$, the drop has been positioned at port i and then both $t_i \geq \frac{L_\mathrm{port}}{v_c}$ and (33) hold. Differently, when $b_i = 0$, $t_i \geq 0$ and $t_i \leq 0$, which makes $t_i = 0$ as such port has not been in contact with the drop. These two inequalities are included in constraints C1 and C2 of the MAXSNR optimization problem detailed in (39). The sum of all time allocated at each port must be a coherence time, which is detailed in constraint C3.

2) Modeling the drop movement throughout the antenna: The initial port where the drop is located is named i_0. Therefore it is known that such a port is pre-selected, i.e., $b_i = 1, \, i = i_0$. This is included as constraint C4 in (39). Now, the drop can move in the left or the right directions to maximize the average SNR. This is modeled by two new binary variables denoted by F_w and B_w, which will take values 1 or 0 if drop moves forward or backward for F_w case, and 1 or 0 if drop moves backward or forward for B_w. Note that the following equality must hold,

$$F_\mathrm{w} + B_\mathrm{w} = 1 \tag{34}$$

which has been included as constraint C5 in (39). If drop is moving to the right, all remaining ports located on the left will not be selected and then their b_i values are zero. Differently, if drop is moving to the left, all remaining ports located on the right will not be selected and then their b_i values are zero. This is modeled by another big-M approach and the following two inequalities

$$b_i \leq M_2 \cdot (1 - F_\mathrm{w}), \forall i < i_0 \tag{35}$$

$$b_i \leq M_2 \cdot (1 - B_\mathrm{w}), \forall i > i_0 \tag{36}$$

that are included as constraints C6 and C7 in (39). In this case $M_2 = 1$ as an upper bound of b_i.

Now, b_i values must be modeled to be taken by ports that are potentially selected by the drop when moving. If moving forward (F_w), consecutive ports must be selected, which is formulated as

$$b_i - b_{i-1} \leq M_2 \cdot (1 - F_\mathrm{w}), \forall i > i_0. \tag{37}$$

Differently, if moving backward (B_w), the inequality is

$$b_{i-1} - b_i \leq M_2 \cdot (1 - B_\mathrm{w}), \forall i < i_0. \tag{38}$$

Note that $b_i - b_{i-1}$ and $b_{i-1} - b_i$ equal 0 when both ports are selected by the drop, or -1 when the drop stops at port $i-1$ or i, respectively. These two inequalities are included as constraints C8 and C9 in (39), respectively.

3) Definition of variables: The rest of the constraints (C10-C14) contain the definition of the unknown variables. Variables $b_i \, \forall i$, F_w and B_w are binary, whereas $t_i \, \forall i$ contain real values between 0 and T_c.

4) Solvable optimization problem: Since the objective functions defined before are linear, our optimization problem can be formulated as a mixed-integer linear programming (MILP) problem. We formulate the MAXSNR optimization problem as

$$\text{MAXSNR:} \max_{\mathbf{b}, F_\mathrm{w}, B_\mathrm{w}, \mathbf{t}} \sum_i \frac{t_i}{T_\mathrm{c}} \Gamma_i \tag{39}$$

$$\begin{aligned}
&\text{subject to} \\
&\mathrm{C1}: \tfrac{L_\mathrm{port}}{v_c} \cdot b_i \leq t_i, \forall i \\
&\mathrm{C2}: t_i \leq M_1 \cdot b_i, \forall i \\
&\mathrm{C3}: \textstyle\sum_i t_i = T_\mathrm{c} \\
&\mathrm{C4}: b_i = 1, \, i = i_0 \\
&\mathrm{C5}: F_\mathrm{w} + B_\mathrm{w} = 1 \\
&\mathrm{C6}: b_i \leq M_2 \cdot (1 - F_\mathrm{w}), \forall i < i_0 \\
&\mathrm{C7}: b_i \leq M_2 \cdot (1 - B_\mathrm{w}), \forall i > i_0 \\
&\mathrm{C8}: b_i - b_{i-1} \leq M_2 \cdot (1 - F_\mathrm{w}), \forall i > i_0 \\
&\mathrm{C9}: b_{i-1} - b_i \leq M_2 \cdot (1 - B_\mathrm{w}), \forall i < i_0 \\
&\mathrm{C10}: b_i \in \{0, 1\}, \, \forall i \\
&\mathrm{C11}: F_\mathrm{w} \in \{0, 1\} \\
&\mathrm{C12}: B_\mathrm{w} \in \{0, 1\} \\
&\mathrm{C13}: t_i \geq 0, \forall \, i \\
&\mathrm{C14}: t_i \leq T_\mathrm{c}, \forall \, i
\end{aligned}$$

Algorithm 1 Port selection based on threshold

Require: i_0, N, T_c, L_port, v_c, $i^* : \Gamma_{i^*} \geq \Gamma_i \forall i$, Γ_m
  $t_\mathrm{i} = 0, \forall i$
  $t_{i_0} = \min(\frac{1}{2}\frac{L_\mathrm{port}}{v_c}, T_\mathrm{c})$
  $T_\mathrm{tot} = \sum_i t_i$
  $i = i_0$
  while $T_\mathrm{tot} < T_\mathrm{c}$ **do**
    if $\Gamma_{i\pm1} \geq \Gamma_\mathrm{m}\,(1 - \vartheta/100)\,\&\, i \neq i^*$ **then**
      $i \leftarrow i \pm 1$
    end if
    if $T_\mathrm{tot} + \frac{L_\mathrm{port}}{v_c} < T_\mathrm{c}$ **then**
      $t_i \leftarrow t_i + \frac{L_\mathrm{port}}{v_c}$
    else
      $t_i \leftarrow t_i + T_\mathrm{c} - T_\mathrm{tot}$
    end if
    $\Gamma_\mathrm{m} = \Gamma_\mathrm{m} + \Gamma_i \frac{L_\mathrm{port}}{T_\mathrm{c} v_c}$,
    $T_\mathrm{tot} = \sum_i t_i$
  end while

Algorithm 2 Port selection based on neighbors comparison

Require: i_0, N, T_c, L_port, v_c, Γ_i
  $t_i = 0, \forall i$
  $t_{i_0} = \min(\frac{3}{2}\frac{L_\mathrm{port}}{v_c}, T_\mathrm{c})$
  $T_\mathrm{tot} = \sum_i t_i$
  while $T_\mathrm{tot} < T_\mathrm{c}$ **do**
    if $i + 1 \leq N\,\&\,\Gamma_{i+1} > \Gamma_i\,\&\,\Gamma_{i+1} > \Gamma_{i-1}$ **then**
      $i \leftarrow i + 1$
    else if $i - 1 \geq 0\,\&\,\Gamma_{i-1} > \Gamma_i\,\&\,\Gamma_{i-1} > \Gamma_{i+1}$ **then**
      $i \leftarrow i - 1$
    end if
    if $T_\mathrm{tot} + \frac{L_\mathrm{port}}{v_c} < T_\mathrm{c}$ **then**
      $t_i \leftarrow t_i + \frac{L_\mathrm{port}}{v_c}$
    else
      $t_i \leftarrow t_i + T_\mathrm{c} - T_\mathrm{tot}$
    end if
    $T_\mathrm{tot} = \sum_i t_i$
  end while

It complies with all features to be solved by a non-convex solver such as Gurobi and CVX interface [28], [30].

B. Threshold-based algorithm

This alternative approach does not require knowledge of the channel at all ports, but only the direction toward the port offering the best SNR. This still corresponds to an ideal scenario, although the amount of CSI required is much smaller than for the previous algorithm. Just as before, an initial sweep is done to start the algorithm in the port with the best SNR. Additionally, during this sweep, the SNR at each port is obtained and averaged. A parameter Γ_m is defined that represents the average of the SNR of the ports that have been selected. It is initialized with the value $\frac{1}{N}\sum_i \Gamma_i$.

Henceforth, each time the drop moves into a new port, its SNR is estimated (Γ_i) and compared to Γ_m. At that point ϑ is defined as a threshold that indicates how much greater than Γ_m the new SNR can be to go to the next port. If the threshold is not overcome, this would imply that the displacement is not compensated by the potential rate gain at the new position. The threshold ϑ is defined as a percentage of Γ_m, hence $\vartheta \in [0, 100]$. The drop would move more frequently if ϑ is low since the threshold would be more restrictive. The antenna remains static for the remaining coherence time, until a new value of Γ_i is detected. By contrast, a high ϑ would impose a softer boundary for the SNR, resulting in more often reconfigurations. Algorithm 1 summarizes the proposed port selection strategy.

Defining ϑ adds a reconfiguration logic into the FA that does not necessarily require a perfect knowledge of CSI. Undoubtedly, the use of a suboptimal threshold through a practical algorithm decreases the overall performance of the FA, since the optimal configuration is usually not achieved. Due to its strong reliance on FA characteristics like drop speed, port spacing, and correlation scenario, it is difficult to find a closed-form expression to obtain this threshold. However, as will be shown below, it can be numerically adapted for particular configurations in accordance with the communications' requirements. Optimizing this procedure and the threshold is not the primary goal of this work and will be addressed in future research.

C. Realistic algorithm

Additionally, a realistic algorithm is proposed, where only the SNRs of ports that are at both sides of the current position of the drop may be known, which can be easily measured in practice. This is detailed in Algorithm 2, and requires to know the starting drop position i_0, the number of ports in which the FA is divided (N), the coherence time (T_c), the length of each port (L_port), the drop speed when moving (v_c) and the SNR values obtained by current and neighboring ports, denoted by Γ_i, Γ_{i-1} and Γ_{i+1}, respectively.

The time spent at the starting drop position i_0 is initialized as the minimum time between $\frac{3}{2}\frac{L_\mathrm{port}}{v_c}$ and T_c. We assume that the drop, at the initial instant, is located at one end of the port and can therefore sense a neighbor without a considerable time loss. Now, it has to cross its own port to sense the other neighbor $\left(\text{travel time: } \frac{L_\mathrm{port}}{v_c}\right)$. Then it makes a decision: whether to move towards that neighbor or towards the other one in case it offered a larger SNR. Consequently, the time to make the first movement will be $\frac{L_\mathrm{port}}{v_c}$ or $2\frac{L_\mathrm{port}}{v_c}$. Since this time depends on the initial position of the drop (at the right-most or left-most port), it is accounted by using $\frac{3}{2}\frac{L_\mathrm{port}}{v_c}$.

While the elapsed time denoted by T_tot does not reach the coherence time T_c, the drop keeps sensing the SNR offered by ports on both sides, and moves to the one offering the larger SNR. Then the elapsed time at such a port i is updated by the time spent on it, computed as the time that a drop takes to cross it (L_port/v_c) or the remaining time to reach T_c.

D. Complexity analysis

Let us evaluate the complexity of the three algorithms. The proposed (MAXSNR) algorithm introduced in Section IV-A is a linear programming problem whose complexity order can be

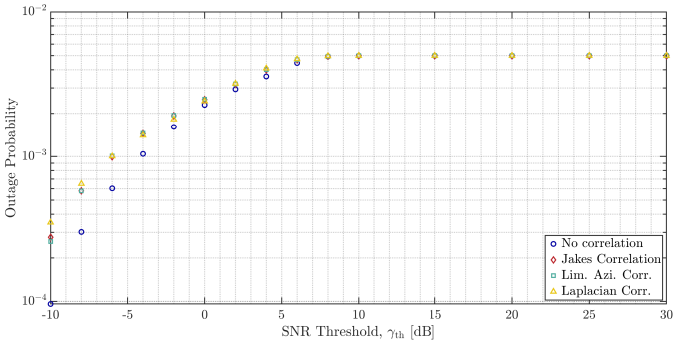

Fig. 5. Outage probability for different correlation scenarios against Γ_{th}.

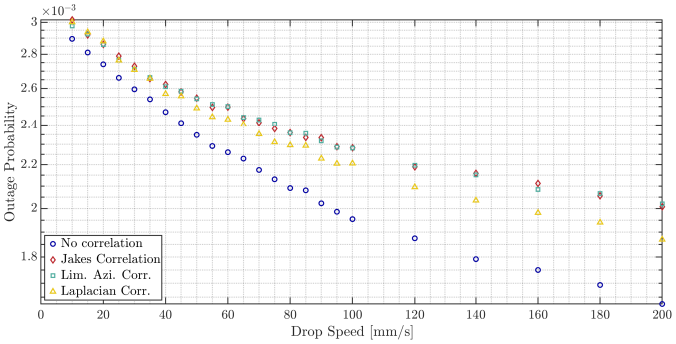

Fig. 6. Outage probability for different correlation scenarios against drop speed.

approximated in practice as $\mathcal{O}(v^2c)$, where v is the number of variables and c is the number of constraints [31]. There are $v = 2N+2$ variables and $c = 6N+1$ constraints in (39), thus the complexity can be approximated as $\mathcal{O}(24N^3) \approx \mathcal{O}(N^3)$.

The proposed threshold-based algorithm detailed in Section IV-B and Algorithm 1 introduces a complexity of $\mathcal{O}(N)$ in the initialization. The *while* loop runs at most $T_{\text{c}}/(L_{\text{port}}v_c)$ times, which is indicated by the increasing step of t_i at each iteration until it reaches T_{c}. At each iteration, the complexity is $\mathcal{O}(N)$, which leads to a complexity of the whole loop of $\mathcal{O}(NT_{\text{c}}/(L_{\text{port}}v_c))$. Then, the total complexity is $\mathcal{O}(N + NT_{\text{c}}/(L_{\text{port}}v_c))$. As T_{c}, L_{port} and v_c are constant, then the complexity could be simplified as $\mathcal{O}(N)$.

The proposed realistic algorithm detailed in Section IV-C and Algorithm 2, although it has different conditional statements, presents the same structure as Algorithm 1. Therefore, its complexity is also $\mathcal{O}(N)$.

V. Performance metrics for FAS

Quantifying the performance of FAS strongly depends on the used modeling techniques. Most authors in the literature compute the OP, defined as the probability of the SNR being below a given threshold Γ_{th} [18]

$$\text{OP} = \Pr\left(\Gamma_i < \Gamma_{\text{th}}\right) \tag{40}$$

However, this OP may not be adequate to fully understand the dynamics of the FA. Figure 5 shows the measured OP of three different correlation scenarios, using the SMD method with parameters later described in Table III. Note that all scenarios offer comparable OP that is near zero. Nonetheless, it can be seen that uncorrelated ports present better outage which is particularly relevant at greater Γ_{th} values.

Figure 6 shows a similar trend. Although there is no significant variation among most of the curves, if the ports are uncorrelated the performance is much better than for the rest of the propagation channel conditions. The performance improves at higher drop speeds, as expected. This result confirms the need for realistic correlation environments to be taken into account. Also, the OP is not completely capturing the channel effects on the performance of the FA, as impractically large values of the reconfiguration speed and Γ_{th} would be needed to obtain the classic OP curve often shown in the literature (that often assumes idealistic conditions).

In light of the above, a different metric is needed to capture the impact of the spatial correlation and appropriately characterize the system performance over time.

We will start from the achievable rate, following Shannon-Hartley theorem, which is expressed as [18]

$$\eta = \log_2(1+\gamma) \quad . \tag{41}$$

Here γ represents a generic SNR that can be measured over different periods of time. As a reminder, Γ_i refers to the instantaneous SNR, and $\bar{\Gamma}$ is the averaged SNR over a coherence time. Consequently, different achievable rates can be defined to analyze each port adaptation algorithm using (41). This enables to define several figures of merit that are summarized in Table II.

Firstly, η^* is defined as the achievable rate of the port with the best SNR, η_{i} as the instantaneous achievable rate of the FA and η_{c} as the average rate over a coherence time. Ideally, the algorithms should keep η_{c} and η_{i} as close as possible to η^* which would imply that the operation is close to the best performance. To measure this gap, we define the instantaneous rate loss

$$\xi_{\text{i}} = \mathbb{E}\left[\frac{\eta^* - \eta_{\text{i}}}{\eta^*}\right] \tag{42}$$

as the difference, in terms of rate, of the port with best SNR and the instantaneous SNR achieved by the FA, expressed as a ratio over η^*. Notably, a lower ξ_{i} value means a better performance. Alternatively, when considering the averaged SNR instead of the instantaneous SNR, we define

$$\xi_{\text{c}} = \mathbb{E}\left[\frac{\eta^* - \eta_{\text{c}}}{\eta^*}\right] \tag{43}$$

with the same implications that were presented above. The motivation for this metric is that maximizing the rate over the coherence time is more practical than working on the instantaneous one.

Yet another metric is defined to evaluate the advantage of reconfiguring the FA, the reconfiguration efficiency ζ, where we compare the rate obtained when reconfiguring the antenna versus the rate obtained when the drop does not move from i_0 post. This metric is defined as

$$\zeta = \mathbb{E}\left[\frac{\eta_{\text{i}} - \eta_{\text{i}_0}}{\eta_{\text{i}_0}}\right] \tag{44}$$

where η_{i_0} denotes the achievable rate of the initial port.

TABLE II
METRIC NOTATION SUMMARY

Parameter	Description
η^*	Achievable rate of the port with best SNR
η_{c}	Coherence time-averaged achievable rate of the FA
η_{i}	Instantaneous achievable rate: achieved by the FA at every time instance
η_{i_0}	Instantaneous achievable rate in the port where the FA was initially configured
ξ_{i}	Instantaneous rate loss: of η_{i} when compared to η^*. See (42)
ξ_{c}	Coherence time-averaged rate loss: between port with best SNR and η_{c} (43)
ζ	Reconfiguration efficiency: rate gain when compared to static antenna scheme as shown in (44)

TABLE III
SIMULATION PARAMETERS OVERVIEW

		General
Montecarlo repetitions	500	-
Simulation length	200	s
Coherence time T_{c}	500	ms
Carrier frequency	3	GHz
σ_h^2	0-20	dB
Γ_{th}	0	dB
μ (block method)	0.97	-
ς_{th} (block method)	1	-
ϑ (threshold algorithm)	0-100	-
		FAS
L	2	wavelengths
Drop speed, v_c	20-100	mm/s
N	40	ports
		Correlation
Δ (Limited azimuth)	$\pi/4$	rad
σ (Laplacian)	48	deg (°)
φ_0 (Laplacian)	67.5	deg (°)

VI. NUMERICAL RESULTS

In this section, several FA correlation models will be applied to evaluate the port selection algorithms in different scenarios, using the proposed metrics. Table III summarizes the general parameters used to obtain the numerical results, where the number of Montecarlo repetitions and simulation length are large enough to ensure statistical consistency. The coherence time is set to 500 ms, unless otherwise specified, representing a considerably static scenario. Drop speed is generally set to 60 mm/s, although it varies from 20 to 100 mm/s when specified. The carrier frequency is set to 3 GHz for a FA of length equal to twice the carrier wavelength consisting of 40 ports. For correlated environments, a limited azimuth of $\pm 45°$ was considered (Δ) and the parameters for the Laplacian model are set to 48° and 67.5° for σ and φ_0 respectively. This implies an AS of 35° [21]. The parameters of the Block model are adjusted to $\mu = 0.97$ and $\varsigma_{\mathrm{th}} = 1$ following the suggestion from [17].

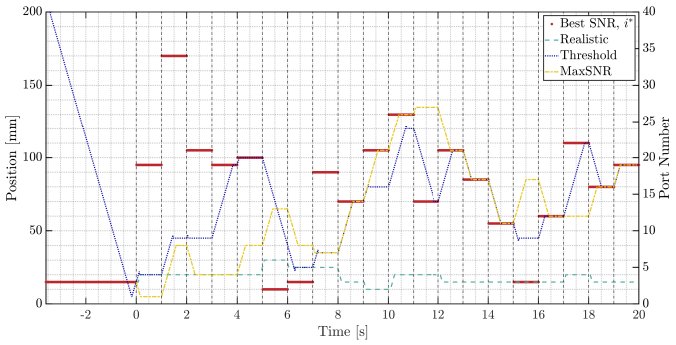

Fig. 7. Overview of the different reconfiguration processes proposed for the FA. Red denotes the port with greater SNR whereas non-solid lines stand for the different strategies. Only 20 different channel values are shown for readability.

The outcome of a typical experimental iteration can be seen in Fig. 7, with a larger coherence time of $T_{\mathrm{c}} = 1$ s. Whereas the port with best SNR is highlighted in red, the other curves denote the position of the drop at every moment for a particular reconfiguration methodology (threshold-based, realistic and MAXSNR). We can observe how, despite starting at the same port, due to their choices over time they ultimately differ in the overall achievable rate. Vertical dashed lines represent the coherence period.

A. Performance of the port selection algorithms

We start by evaluating the performance of the different proposed algorithms. Figure 8 plots the rate loss metrics when the ports are uncorrelated. The MAXSNR algorithm undoubtedly performs best. Nevertheless, higher v_c benefits the threshold algorithm over the realistic one. This is due to the fact that the drop will be placed at i^* for a longer time, and the lower achieved rates while the drop moves are compensated by the gain achieved at i^*. The same trend is expected when using ζ, as can be seen in Fig. 9. As expected, for higher reconfiguration speeds, the overall performance of the FA is better, as shown by all curves. Interestingly, realistic and optimal algorithms do not present the same tendency along the whole drop speed range. There is a crossing point at approximately 65 mm/s in this scenario. This is explained by the fact that the threshold algorithm always moves the drop toward i^*. Should the drop speed be large, the drop would arrive faster and outperform the realistic algorithm by far.

We address now the choice of the value of ϑ for the threshold-based algorithm. Figure 10 illustrates how ξ_{c} changes as a function of the value of the threshold for two different values of $v_c = 40$ mm/s and $v_c = 80$ mm/s, denoted as slow and fast respectively. Four different correlation scenarios are shown. Remarkably, faster drop speeds have a greater impact on the choice for ϑ whereas it is not as critical for lower speeds. Furthermore, the correlation environments play an important role as compared to the scenario with no correlation.

The same qualitative results can be observed in Fig. 11, where reconfiguration efficiency is plotted for different correlation scenarios and speeds. Notably, the choice of ϑ does not

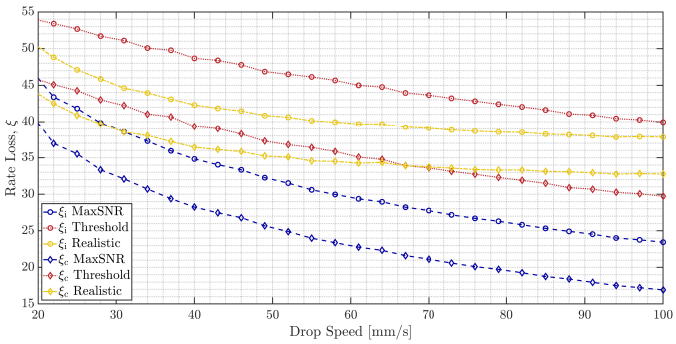

Fig. 8. Different rate loss metrics, ξ, against drop speed, for uncorrelated ports: threshold-based, realistic and MAXSNR.

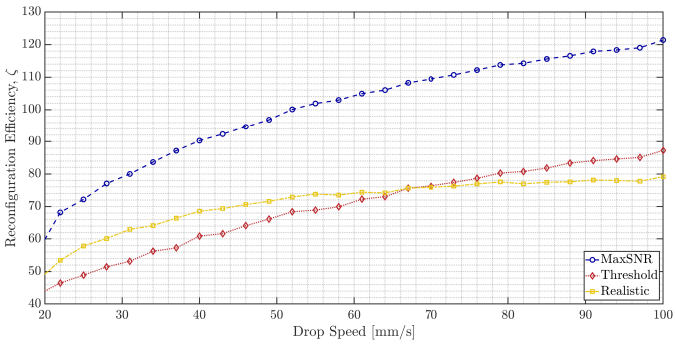

Fig. 9. Reconfiguration efficiency metric, ζ, against drop speed for uncorrelated ports: threshold-based, realistic and MAXSNR.

seem to have an influence on the uncorrelated ports scenario at low drop speeds.

Figure 12 works in a similar fashion: it shows the instantaneous rate loss for different correlation scenarios with two distinct number of ports. It can be seen how the increase in the number of ports does not necessarily improve the performance, as will be discussed during next subsection.

After evaluating these former results, $\vartheta > 80$ seems to be convenient for the scenarios under study. Therefore we are generally using $\vartheta = 90$ for further results, as stated in Table III. This implies that newer SNR values must be close to Γ_{m} for the drop to move without loosing performance.

B. Effect of port densification

In Fig. 13 we show the effect of port densification. At first sight, it may seem that the greater the number of ports, the better the spatial diversity, hence better performance. Nonetheless, spatial correlation significantly reduces diversity. We can see that it is impractical to consider more than 10 - 15 ports per wavelength since no better capabilities are achieved, while the associated hardware complexity (not directly addressed in this work) would increase. Furthermore, for some scenarios and algorithms (such as the one in Fig. 12), a high number of ports may lead to a performance worsening due to the lower achieved rates while reconfiguring the FA. Hence, the parameters of the FAS (drop speed, port number) should change to improve reconfiguration efficiency.

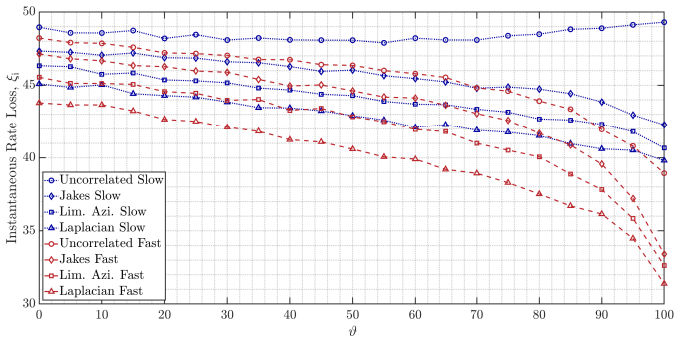

Fig. 10. Instantaneous rate loss for different values of ϑ (threshold-based algorithm) under different correlation scenarios for two different speeds: $v_d = 40$ mm/s and $v_d = 80$ mm/s, denoted as slow and fast respectively.

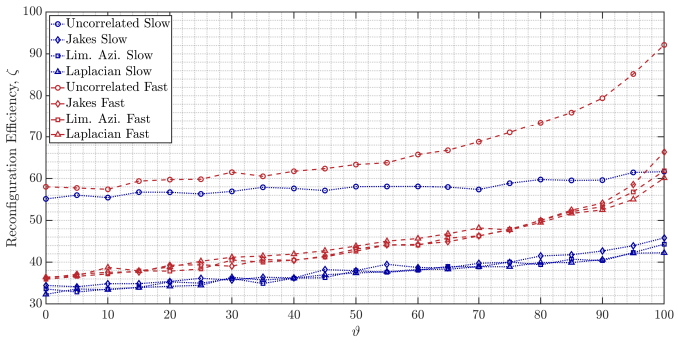

Fig. 11. Reconfiguration efficiency for different values of ϑ (threshold-based algorithm) under different correlation scenarios for two different speeds: $v_d = 40$ mm/s and $v_d = 80$ mm/s, denoted as slow and fast respectively.

C. Impact of correlation

The following figures show the impact of the correlation and the differences among the proposed correlation modeling techniques. Fig. 14 plots the metric ξ_{c} using the realistic port selection technique in different correlated environments. Higher values of, σ_h^2, lead to smaller differences in the metric, as there would be smaller SNR differences between any position and i^*. Hence, the reconfiguration capability is clearly more advantageous in low SNR scenarios.

Figure 15 shows that similar results are obtained for the realistic reconfiguration algorithm when evaluated using the ARMA, SMD and Block correlation modeling techniques. Under the Jakes' model, the three models show similarly that the performance is worse than in the uncorrelated case. In the case of limited azimuth, the performance when the Block method is used slightly deviates with respect to the other two models. We hypothesize that this behavior is produced because its parameters have not been particularized in [17] to the limited azimuth case, but they were set to match Jakes' model instead.

VII. CONCLUSIONS

In this paper, with focus on advancing the use of liquid antennas for FAS, a thorough analysis of correlation modeling state of art has been conducted. Three different modeling techniques have been presented, with special attention paid to the model accuracy as well as to its numerical complexity

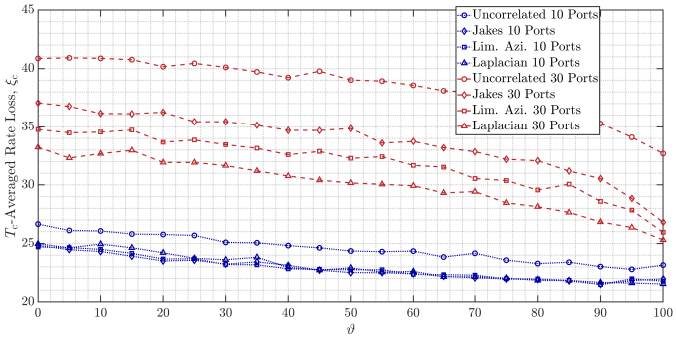

Fig. 12. Coherence-time-averaged rate loss for different values of ϑ under different correlation scenarios for two different numbers of port: $N = 10$ and $N = 30$.

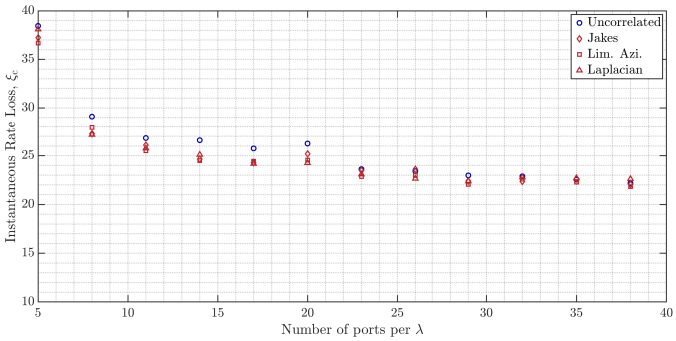

Fig. 13. Effect of port densification in the FA: ξ_c when incrementing the number of ports within a wavelength, for four correlation scenarios.

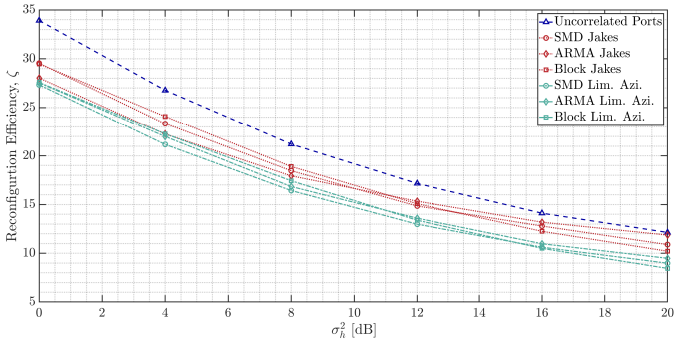

Fig. 14. Reconfiguration efficiency (ζ) for different correlation scenarios and different modeling tools.

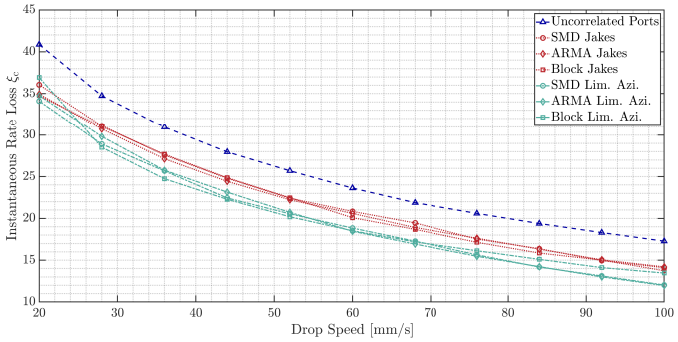

Fig. 15. ξ_c for different correlation scenarios using threshold-based methodology.

and mathematical tractability. They can be used to represent the effects of spatial correlation on the FAS performance. A specific metric has been used to characterize both the reconfiguration speed and the impact of the correlation on the performance of the FA. These parameters encompass a wide range of options that should be investigated to explore the viability of FAS, in addition to other well-known metrics such as the OP. Moreover, for the specific topology under study, the impact of the reconfiguration speed has been discussed. Not being considered in previous work, it was shown that the movement speed of the drop plays a major role in the performance of the system. As a result, it must be taken into consideration in future research on the subject.

Three different algorithms have been proposed addressing port selection for the reconfiguration of the FA. From maximizing the SNR to a more realistic approach requiring milder CSI knowledge, the performance boundaries for FA were discussed, showing the importance of the correlation. Nonetheless, we are still working on a feasible framework to move the drop in a more realistic manner in a FAS testbed. This work contributes to keep advancing FAS as enabling technologies for the upcoming generations of communication systems.

REFERENCES

[1] K.-K. Wong, A. Shojaeifard, K.-F. Tong, and Y. Zhang, "Fluid Antenna Systems," *IEEE Transactions on Wireless Communications*, vol. 20, no. 3, pp. 1950–1962, 2021.

[2] L. Zhu, W. Ma, and R. Zhang, "Movable Antennas for Wireless Communication: Opportunities and Challenges," *IEEE Communications Magazine*, vol. 62, no. 6, pp. 114–120, 2024.

[3] M. D. Dickey, R. C. Chiechi, R. J. Larsen, E. A. Weiss, D. A. Weitz, and G. M. Whitesides, "Eutectic Gallium-Indium (EGaIn): A Liquid Metal Alloy for the Formation of Stable Structures in Microchannels at Room Temperature," *Advanced Functional Materials*, vol. 18, no. 7, pp. 1097–1104, 2008.

[4] J. D. Vega-Sánchez, A. E. López-Ramírez, L. Urquiza-Aguiar, and D. P. M. Osorio, "Novel Expressions for the Outage Probability and Diversity Gains in Fluid Antenna System," *IEEE Wireless Communications Letters*, vol. 13, no. 2, pp. 372–376, 2024.

[5] J. Otero Martínez, J. R. Rodríguez, Y. Shen, K.-F. Tong, K.-K. Wong, and A. G. Armada, "Toward Liquid Reconfigurable Antenna Arrays for Wireless Communications," *IEEE Communications Magazine*, vol. 60, no. 12, pp. 145–151, 2022.

[6] W. K. New, K.-K. Wong, H. Xu, K.-F. Tong, and C.-B. Chae, "An Information-Theoretic Characterization of MIMO-FAS: Optimization, Diversity-Multiplexing Tradeoff and q -Outage Capacity," *IEEE Transactions on Wireless Communications*, vol. 23, no. 6, pp. 5541–5556, 2023.

[7] W. Ma, L. Zhu, and R. Zhang, "Multi-Beam Forming With Movable-Antenna Array," *IEEE Communications Letters*, vol. 28, no. 3, pp. 697–701, 2024.

[8] A. Shojaeifard, K.-K. Wong, K.-F. Tong, Z. Chu, A. Mourad, A. Haghighat, I. Hemadeh, N. T. Nguyen, V. Tapio, and M. Juntti, "MIMO Evolution Beyond 5G Through Reconfigurable Intelligent Surfaces and Fluid Antenna Systems," *Proceedings of the IEEE*, pp. 1–22, 2022.

[9] W. K. New, K.-K. Wong, H. Xu, K.-F. Tong, C.-B. Chae, and Y. Zhang, "Fluid Antenna System Enhancing Orthogonal and Non-Orthogonal Multiple Access," *IEEE Communications Letters*, vol. 28, no. 1, pp. 218–222, 2024.

[10] C. Wang, G. Li, H. Zhang, K.-K. Wong, Z. Li, D. W. K. Ng, and C.-B. Chae, "Fluid Antenna System Liberating Multiuser MIMO for ISAC via Deep Reinforcement Learning," *IEEE Transactions on Wireless Communications*, vol. 23, no. 9, pp. 10879–10894, 2024.

[11] W. K. New, K.-K. Wong, H. Xu, C. Wang, F. R. Ghadi, J. Zhang,

J. Rao, R. Murch, P. Ramírez-Espinosa, D. Morales-Jimenez, C.-B. Chae, and K.-F. Tong, "A Tutorial on Fluid Antenna System for 6G Networks: Encompassing Communication Theory, Optimization Methods and Hardware Designs," *IEEE Communications Surveys & Tutorials*, pp. 1–1, 2024.

[12] M. Wang, C. Trlica, M. R. Khan, M. D. Dickey, and J. J. Adams, "A reconfigurable liquid metal antenna driven by electrochemically controlled capillarity," *Journal of Applied Physics*, vol. 117, no. 19, p. 194901, 2015.

[13] A. Dey, R. Guldiken, and G. Mumcu, "Microfluidically Reconfigured Wideband Frequency-Tunable Liquid-Metal Monopole Antenna," *IEEE Transactions on Antennas and Propagation*, vol. 64, no. 6, pp. 2572–2576, 2016.

[14] R. C. Gough, A. M. Morishita, J. H. Dang, W. Hu, W. A. Shiroma, and A. T. Ohta, "Continuous Electrowetting of Non-toxic Liquid Metal for RF Applications," *IEEE Access*, vol. 2, pp. 874–882, 2014.

[15] J. Otero Martinez and A. G. Armada, "Realistic Correlation Modeling for Fluid Antenna Systems," in *2024 IEEE International Conference on Communications Workshops (ICC Workshops)*, pp. 1371–1376, 2024.

[16] A. M. Morishita, C. K. Y. Kitamura, A. T. Ohta, and W. A. Shiroma, "A Liquid-Metal Monopole Array With Tunable Frequency, Gain, and Beam Steering," *IEEE Antennas and Wireless Propagation Letters*, vol. 12, pp. 1388–1391, 2013.

[17] P. Ramirez-Espinosa, D. Morales-Jimenez, and K.-K. Wong, "A New Spatial Block-Correlation Model for Fluid Antenna Systems," *IEEE Transactions on Wireless Communications*, vol. 23, no. 11, pp. 15829–15843, 2024.

[18] A. Goldsmith, *Wireless Communications*. Cambridge University Press, 2005.

[19] W. C. Jakes, *Microwave Mobile Communications*. Piscataway, NJ: IEEE Press, 1994.

[20] R. H. Clarke, "A statistical theory of mobile-radio reception," *The Bell System Technical Journal*, vol. 47, no. 6, pp. 957–1000, 1968.

[21] 3GPP, "Spatial channel model for multiple input multiple output (MIMO) simulations (v18.0.0)," Tech. Rep. TR 25.996, 3rd Generation Partnership Project, 2024.

[22] P. Teal, T. Abhayapala, and R. Kennedy, "Spatial correlation for general distributions of scatterers," *IEEE Signal Processing Letters*, vol. 9, no. 10, pp. 305–308, 2002.

[23] M. C. Jeruchim, Balaban, Philip, and K. S. Shanmugan, eds., *Simulation of Communication Systems: Modeling, Methodology, and Techniques*. Information Technology–Transmission, Processing, and Storage, New York: Kluwer Academic/Plenum Publishers, 2nd ed ed., 2000.

[24] C. E. Rasmussen and C. K. I. Williams, *Gaussian Processes for Machine Learning*. Adaptive Computation and Machine Learning, Cambridge, Mass.: MIT Press, 3. print ed., 2008.

[25] B. Friedlander and B. Porat, "The Modified Yule-Walker Method of ARMA Spectral Estimation," *IEEE Transactions on Aerospace and Electronic Systems*, vol. AES-20, no. 2, pp. 158–173, 1984.

[26] S. Kay and S. Marple, "Spectrum analysis—A modern perspective," *Proceedings of the IEEE*, vol. 69, no. 11, pp. 1380–1419, 1981.

[27] W. K. New, K.-K. Wong, H. Xu, F. R. Ghadi, R. Murch, and C.-B. Chae, "Channel Estimation and Reconstruction in Fluid Antenna System: Oversampling is Essential," *IEEE Transactions on Wireless Communications*, vol. 24, no. 1, pp. 309–322, 2025.

[28] Gurobi Optimization, LLC, "Gurobi Optimizer Reference Manual," 2023.

[29] D. G. Luenberger and Y. Ye, *Linear and Nonlinear Programming*. Springer Publishing Company, Incorporated, 2015.

[30] M. Grant and S. Boyd, "CVX: Matlab software for disciplined convex programming, version 2.1." http://cvxr.com/cvx, Mar. 2014.

[31] S. Boyd and L. Vandenberghe, *Convex Optimization*. Cambridge University Press, 2004.

JAVIER OTERO MARTINEZ received the B.Sc. in Telecommunications Engineering in 2019 from the Universidad Politécnica de Madrid and two M.Sc. in Telecommunications Engineering and Advanced Communications Technologies from the Universidad Carlos III de Madrid in 2021. There, he is currently pursuing his PhD within the Department of Signal Theory and Communications, focused on physical layer technologies. His current research interests are related to liquid antennas; materials, performance, prototyping and modeling.

BORJA GENOVES GUZMAN (Senior Member, IEEE) received a B.Sc. degree from Universidad Carlos III de Madrid, Spain, in 2013, a double M.Sc. degree (Hons.) in electrical engineering from Universidad Carlos III de Madrid, and the Institut Mines-Télécom, France, in 2015, and a Ph.D. degree from University Carlos III of Madrid in 2019 (Extraordinary Ph.D. award). He received the First Prize in Graduation National Awards by the Ministry of Education, Culture and Sports from Spain. He worked as a postdoctoral researcher for 3 years at IMDEA Networks Institute. He has carried out research stays at University of Virginia (USA) - 2 years, University of Southampton (UK) - 3 months and The University of Edinburgh (UK) - 3 months. He is currently working as a Marie Skłodowska-Curie Actions Postdoctoral Global Fellow in Universidad Carlos III de Madrid, and starting as a Ramón y Cajal researcher from September 2025. He has published over 45 peer-reviewed contributions. He also holds 2 patents (1 submitted and 1 granted). His research career has been supported by 3 regional, 3 national, and 5 European research projects, 2 of them as Principal Investigator. His research interests are visible light communication (also referred to as LiFi), Internet of Things (IoT) and low-power wireless communications.

ANA GARCÍA ARMADA is an IEEE Fellow. She is a Professor at Universidad Carlos III de Madrid. She has been a visiting scholar at Stanford University, Bell Labs, and University of Southampton. She has published more than 250 papers in conferences and journals and she holds six patents. She serves on the editorial boards of IEEE Open Journal of the Communications Society and ITU Journal on Future and Evolving Technologies. She has been a member of the organizing committee of several conferences, including General Chair of IEEE Globecom 2021 and IEEE MeditCom 2024. She has received several awards from UC3M, the third place Bell Labs Prize 2014, the outstanding service award from the IEEE ComSoc Signal Processing and Communications Electronics technical committee and the outstanding service award from the IEEE ComSoc Women in Communications Engineering standing committee. She received the IEEE ComSoc/KICS Exemplary Global Service Award in 2022. Her research focuses mainly on signal processing applied to wireless communications.